PHOTONICS Research

Extreme single-excitation subradiance from two-band Bloch oscillations in atomic arrays

Luojia Wang,[1] Da-Wei Wang,[2] Luqi Yuan,[1,6] Yaping Yang,[3,7] and Xianfeng Chen[1,4,5,8]

[1]State Key Laboratory of Advanced Optical Communication Systems and Networks, School of Physics and Astronomy, Shanghai Jiao Tong University, Shanghai 200240, China
[2]Interdisciplinary Center for Quantum Information and State Key Laboratory of Modern Optical Instrumentation, Zhejiang Province Key Laboratory of Quantum Technology and Device, and School of Physics, Zhejiang University, Hangzhou 310027, China
[3]MOE Key Laboratory of Advanced Micro-Structured Materials, School of Physics Science and Engineering, Tongji University, Shanghai 200092, China
[4]Shanghai Research Center for Quantum Sciences, Shanghai 201315, China
[5]Collaborative Innovation Center of Light Manipulations and Applications, Shandong Normal University, Jinan 250358, China
[6]e-mail: yuanluqi@sjtu.edu.cn
[7]e-mail: yang_yaping@tongji.edu.cn
[8]e-mail: xfchen@sjtu.edu.cn

Received 21 September 2023; revised 26 November 2023; accepted 30 December 2023; posted 3 January 2024 (Doc. ID 506450); published 1 March 2024

Atomic arrays provide an important quantum optical platform with photon-mediated dipole–dipole interactions that can be engineered to realize key applications in quantum information processing. A major obstacle for such applications is the fast decay of the excited states. By controlling two-band Bloch oscillations of single excitation in an atomic array under an external magnetic field, here we show that exotic subradiance can be realized and maintained with orders of magnitude longer than the spontaneous decay time in atomic arrays with the finite size. The key finding is to show a way for preventing the wavepacket of excited states scattering into the dissipative zone inside the free space light cone, which therefore leads to the excitation staying at a subradiant state for an extremely long decay time. We show that such operation can be achieved by introducing a spatially linear potential from the external magnetic field in the atomic arrays and then manipulating interconnected two-band Bloch oscillations along opposite directions. Our results also point out the possibility of controllable switching between superradiant and subradiant states, which leads to potential applications in quantum storage.

https://doi.org/10.1364/PRJ.506450

1. INTRODUCTION

Light–matter interaction in subwavelength scale is of broad interest in quantum information processing and quantum metrology [1,2]. Such interactions in subwavelength atomic arrays [3–28] can induce long-range nonlinear dipole–dipole interactions by mediating photons in radiation modes [3,5,29,30] or via long-range van der Waals interactions between Rydberg states [31]. Further controls of atomic arrays by magnetic fields bring remarkable physical phenomena, including super- and subradiant states [32], photon storage and retrieval [33–35], subradiance-protected quantum state transport [36], and many others [37–45]. These quantum information processing methods utilize subradiant quantum states with inhibited spontaneous decay and exhibit useful applications in quantum storage [46]. Previous research shows that single-excitation subradiant states in one-dimensional (1D) arrays of N atoms typically have decay rates scaling as N^{-3} with a lifetime of 7 orders of magnitude greater than that of a single atom for $N \sim 200$ [6,11,15]. Nevertheless, it generally desires a quantum state lasting long enough for the purpose of quantum storage [46]. A challenging problem is that subradiant states can diffuse into the superradiant subspace through the interaction or boundary effect, which limits their applications in quantum information processing.

Here we show that a judicious coherent control of finite-size atomic arrays can prevent single-excitation subradiant states from entering the superradiant subspace and thus realize subradiance with a lifetime of orders of magnitude longer than that of a single atom with the help of an external magnetic field. Specifically, we consider a well-established model with atomic arrays under the magnetic field, which lifts the degeneracy of excited states in each atom through the Zeeman shift (labeled as $|+\rangle$ and $|-\rangle$) [37,38,41]. Such systems with an infinite size can support subradiant collective excited states outside of the dissipative zone in the momentum space [6,11,15]. However, for

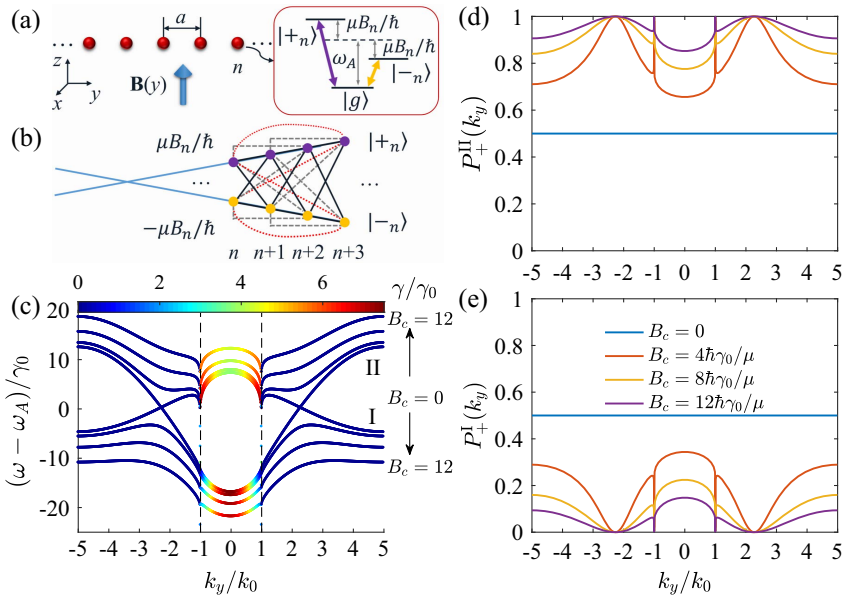

Fig. 1. (a) Schematic of a 1D V-type atomic array under a magnetic field $B(y)$. (b) Schematic of the corresponding lattice where the nth atom has non-degenerate excited states $|\pm_n\rangle$ with frequency shifted by $\pm\mu B_n/\hbar$. Blue lines indicate a linear trend of B_n as in Eq. (2). (c) Band structures with different constant magnetic fields B_c with values $B_c = 0, 4\hbar\gamma_0/\mu, 8\hbar\gamma_0/\mu, 12\hbar\gamma_0/\mu$, respectively. Black arrows indicate values of B_c for corresponding bands. Decay rates of modes are color coded. Probabilities of eigenstates on (d) band II and (e) band I projected on $|+\rangle$ states for different B_c. Here, $a = 0.1\lambda$.

the same system with a finite size, such excitation inevitably spreads to the boundaries and the wavepacket gets scattered into the dissipative zone. To overcome such obstacles, we instead apply a spatially linear magnetic field, which brings linear potentials with opposite slopes on $|+\rangle$ and $|-\rangle$ states [see Fig. 1(b)]. Similar 1D lattices under linear potentials support Bloch oscillations [47–58]. Fundamentally different from the previous work, Bloch oscillations in atomic arrays under a linear magnetic field support two-band Bloch oscillations with interband interactions such that the wavepacket of excited states oscillates on two bands along opposite directions alternatively. This unique picture can force the wavepacket spatially localized within a few atoms while preventing the excitation from entering into the dissipative zone. Hence it supports subradient oscillations surviving extremely long time with finite atoms. We also show the way of switching between superradiant and subradiant oscillations by tuning the external magnetic field, which provides the opportunity for reading out information from subradiant quantum states [59–62].

2. MODEL

The developments of state-of-the-art technologies in various experimental platforms such as trapped neutral atoms at the subwavelength scale [19–28,63–68] pave the way for exploring exotic phenomena in atomic arrays. We study such arrays of atoms that are equally spaced at a distance a along the y-axis [$y_n = na$ for the nth atom in Fig. 1(a)]. Each atom has a ground state $|g\rangle$ and degenerate excited states. We apply an off-plane magnetic field $B(y)$ in the z-direction to lift the degeneracy of two excited states $|\pm\rangle$. Under the single-excitation limit, the dynamics of the wave packet of the excited states is described by the non-Hermitian Hamiltonian after integrating out photonic modes [37,38,41],

$$\begin{aligned} H_{\mathrm{eff}} = \hbar \sum_{n=1}^{N} \sum_{\alpha=\pm} \left(\omega_A - i\frac{\gamma_0}{2}\right) |\alpha_n\rangle\langle\alpha_n| \\ + \sum_{n=1}^{N} \mu B_n (|+_n\rangle\langle+_n| - |-_n\rangle\langle-_n|) \\ + \frac{3\pi\hbar\gamma_0 c}{\omega_A} \sum_{n\neq m} \sum_{\alpha,\beta=\pm} G_{\alpha\beta}(y_n - y_m) |\alpha_n\rangle\langle\beta_m|, \end{aligned} \tag{1}$$

where ω_A is the atomic transition frequency, γ_0 is the atomic decay rate in the free space, $\mu B_n/\hbar$ is the Zeeman shift for the nth atom with the magnetic moment μ, and $G_{\alpha\beta}(y_n - y_m)$ is the free-space dyadic Green's function describing the electric field at y_n emitted by the atom located at y_m. With the relation $|\pm\rangle = \mp(|x\rangle \pm i|y\rangle)/\sqrt{2}$, one obtains $G_{++} = G_{--} = -e^{ik_0 r} \cdot (k_0^2 r^2 - ik_0 r + 1)/(8\pi k_0^2 r^3)$ and $G_{+-} = G_{-+} = e^{ik_0 r}(k_0^2 r^2 + 3ik_0 r - 3)/(8\pi k_0^2 r^3)$, where $r = |y_n - y_m|$ and $k_0 = \omega_A/c = 2\pi/\lambda$ with λ being the wavelength and c being the vacuum speed of light [38,41]. Equation (1) shows a tight-binding lattice model where excitations on sites at two arms ($|\pm\rangle$) have on-site potentials $V_{\pm,n} \equiv \pm\mu B_n$ and are connected by complex and long-range photon-mediated hoppings. In particular, we consider the magnetic field

$$B_n = nB_0, \tag{2}$$

where B_0 is a constant. Equation (2) gives $V_{\pm,n} = \pm n\mu B_0$, which leads to the effective constant force $F_\pm = \mp\mu B_0/a$ in opposite directions on the two excited states. Two effective electric fields in opposite directions on two separated arms in the lattice bring Bloch oscillations on two arms exhibiting

symmetric patterns. However, once the two arms are connected [by terms including $G_{\pm\mp}$ in Eq. (1)], the dynamics of the Bloch-oscillation wavepackets on the two arms is influenced by each other, which can be analyzed in the field-free Bloch band picture.

We first study the band structure of the infinite atomic arrays with constant magnetic field B_c [37,38]. The single-excitation Bloch modes are given by

$$|\Psi_{k_y}\rangle = \sum_n (C_{+,k_y}|+_n\rangle + C_{-,k_y}|-_n\rangle)e^{ik_y na} = (\,C_{+,k_y} \quad C_{-,k_y}\,)^T, \tag{3}$$

where k_y is the Bloch wave vector. The Hamiltonian in the momentum space on two arms has the form

$$\frac{H_k}{\hbar} = \begin{pmatrix} \omega_A - i\frac{\gamma_0}{2} + \chi_{k_y}^{++} & \chi_{k_y}^{+-} \\ \chi_{k_y}^{-+} & \omega_A - i\frac{\gamma_0}{2} + \chi_{k_y}^{--} \end{pmatrix} + \begin{pmatrix} i\frac{\mu B_0}{\hbar a}\frac{\mathrm{d}}{\mathrm{d}k_y} & 0 \\ 0 & -i\frac{\mu B_0}{\hbar a}\frac{\mathrm{d}}{\mathrm{d}k_y} \end{pmatrix}, \tag{4}$$

where $\chi_{k_y}^{\alpha\beta} = \frac{3\pi\gamma_0 c}{\omega_A}\sum_{n\neq 0} e^{ik_y na}\, G_{\alpha\beta}(na)$ and diagonalization of the first term plus the shifts caused by the constant magnetic field gives the two-band structure. Our results show that the oscillatory mode for an extended Gaussian distribution of the single-excitation wavepacket approximately evolves in a single band. The second term in Eq. (4) would transform the distribution on one band into two bands and gives the acceleration force in one band and the tunneling strength to the other band, which surpasses the former one if the two arms have comparable probabilities. We thus bring in a phenomenological force averaging on two arms, $\langle F\rangle \equiv \frac{\mu B_0}{a}\sum_n \langle\Psi|(|+_n\rangle\langle+_n| - |-_n\rangle\langle-_n|)|\Psi\rangle = \frac{\mu B_0}{a}\sum_n (P_+ - P_-)$, to estimate the acceleration force.

We choose $a = 0.1\lambda$, which brings the first Brillouin zone $k_y \in [-5k_0, 5k_0]$. We plot band structures in k_y-space for different B_c in Fig. 1(c). For each B_c, there are two bands, and it exhibits large collective decay, i.e., the dissipative zone in the free-space light cone ($|k_y| < k_0$). Outside of the dissipative zone, subradiant states are supported. For $B_c = 0$, there are two degenerate points near $k_y = \pm 2.3k_0$, while two bands are separated in the entire k_y-space for other B_c. We denote the lower (upper) band as band I (II) and define $P_\pm^{\mathrm{I(II)}}$ as the probability intensity of an eigenstate on band I (II) projected onto the arm of $|\pm\rangle$ states. P_+^{II} and P_+^{I} are shown in Figs. 1(d) and 1(e), respectively. One notes that $P_+^{\mathrm{I(II)}} + P_-^{\mathrm{I(II)}} = 1$. When there is no magnetic field, $P_\pm^{\mathrm{I}} = P_\pm^{\mathrm{II}} = 0.5$ in the entire k_y-space, indicating that probabilities for exciting $|\pm\rangle$ states are equivalent due to the degeneracy of $|\pm\rangle$. However, for $m \neq 0$, it shows asymmetric distributions of $P_\pm^{\mathrm{I(II)}}$. In particular, for $B_c > 0$ on band I (II), we can see that $P_+^{\mathrm{I}} < 0.5$ ($P_+^{\mathrm{II}} > 0.5$), meaning that less (more) density of the state is located on the arm of $|+\rangle$ states. Distributions of $P_\pm^{\mathrm{I(II)}}$ are highly symmetric because the influence of $|\pm\rangle$ is symmetric under the positive/negative magnetic field. Moreover, we find that, for $B_c > 0$ at $k_y = \pm 2.3k_0$, it shows $P_+^{\mathrm{I}} = 0$ ($P_+^{\mathrm{II}} = 1$) on band I (II). We note that band structures in Fig. 1 are calculated by simply summing the Green's function in real space over all lattice sites, which artificially induces the inaccurate eigenvalues at k_y near $\pm k_0$ in the free-space light cone due to slow convergence. However, this inaccuracy in band structures does not affect the later analysis throughout this paper. Also, if desired, it can be overcome by summations of Green's function in momentum space with an appropriate regularizing method [37,38].

We next introduce the simulation method for studying the dynamics of the single excitation wavepacket in the atomic arrays. We use the Schrödinger equation $\mathrm{d}|\Psi(t)\rangle/\mathrm{d}t = -iH_{\mathrm{eff}}|\Psi(t)\rangle/\hbar$ and the excitation wavepacket of the atomic array $|\Psi(t)\rangle = \sum_n [C_{+,n}(t)|+_n\rangle + C_{-,n}(t)|-_n\rangle]e^{-i\omega_A t}$, where $|C_{\pm,n}|^2$ gives the excitation probability of the $|\pm\rangle$ state in the nth atom. Two hundred one atoms ($n = -100, \ldots, 0, \ldots, 100$) are considered in the arrays. $B_0 = 0.2\hbar\gamma_0/\mu$ is used in simulations. We assume that the wavepacket of the system is initially prepared at a superposition state on two arms following $C_{\pm,n}(0) = \psi_\pm \exp[ik_c an - (n-n_c)^2/200]$, where n_c is the spatial center of the initial excitation, k_c is the initial momentum, and $\psi_\pm$ gives the initial ratio of excitation amplitudes on two arms of the $|\pm\rangle$ states. Such an initial state in the weak excitation limit can be pumped with phase-controlled schemes [32,33,59,69] or by applying a spatial modulation of the atomic detuning [18].

3. RESULTS

For finite atomic arrays, the key ingredient for maintaining a long-standing subradiant state is to prevent the wavepacket from entering into the dissipative zone either by oscillations or scattering due to the boundary effects. One might notice that the well-established Bloch oscillation may lead the wavepacket oscillation within a finite spatial region and propagating unidirectionally in the k_y-space [50,53,70], so by frequently altering the direction of the constant force, it is possible to accomplish the task for avoiding entering the dissipative zone. Nevertheless, here we show that one can realize such a task in atomic arrays under a spatially linear but temporally constant magnetic field [Eq. (2)], which leads to effective constant forces in opposite directions on the two excited states. Once the two arms are connected via photon-mediated dipole–dipole interactions, the effective electric force that acts on the single-excitation wavepacket depends on the wavepacket distributions between the two arms. Our results show that an extended Gaussian distribution of the single-excitation wavepacket approximately evolves in a single band driven by the phenomenological force $\langle F\rangle$, which can be estimated by the eigenstate distributions of the moving wavepacket in a band structure under a constant magnetic field felt by the wavepacket center. The ability of altering the effective force direction during Bloch oscillations provides the mechanism to build subradiant states that avoid entering the dissipative zone inside the free-space light cone and are spatially localized far away from the boundary of the finite array.

To see the long-standing subradiant state, we excite the wavepacket centered at $n = 0$, i.e., $n_c = 0$, with $\psi_+ = \psi_- = 0.168$ and $k_c = 1.5k_0$, which satisfies $\sum_n[|C_{+,n}(0)|^2 + |C_{-,n}(0)|^2] = 1$. The evolutions in the simulation are plotted for the time up to $10T_B$, where $T_B = 2\pi\hbar/\mu B_0 = 10\pi/\gamma_0$. Figures 2(a1) and 2(b1) depict the dynamics of $|C_{+,n}(t)|^2$ and $|C_{-,n}(t)|^2$, respectively, and one sees a sustained Bloch

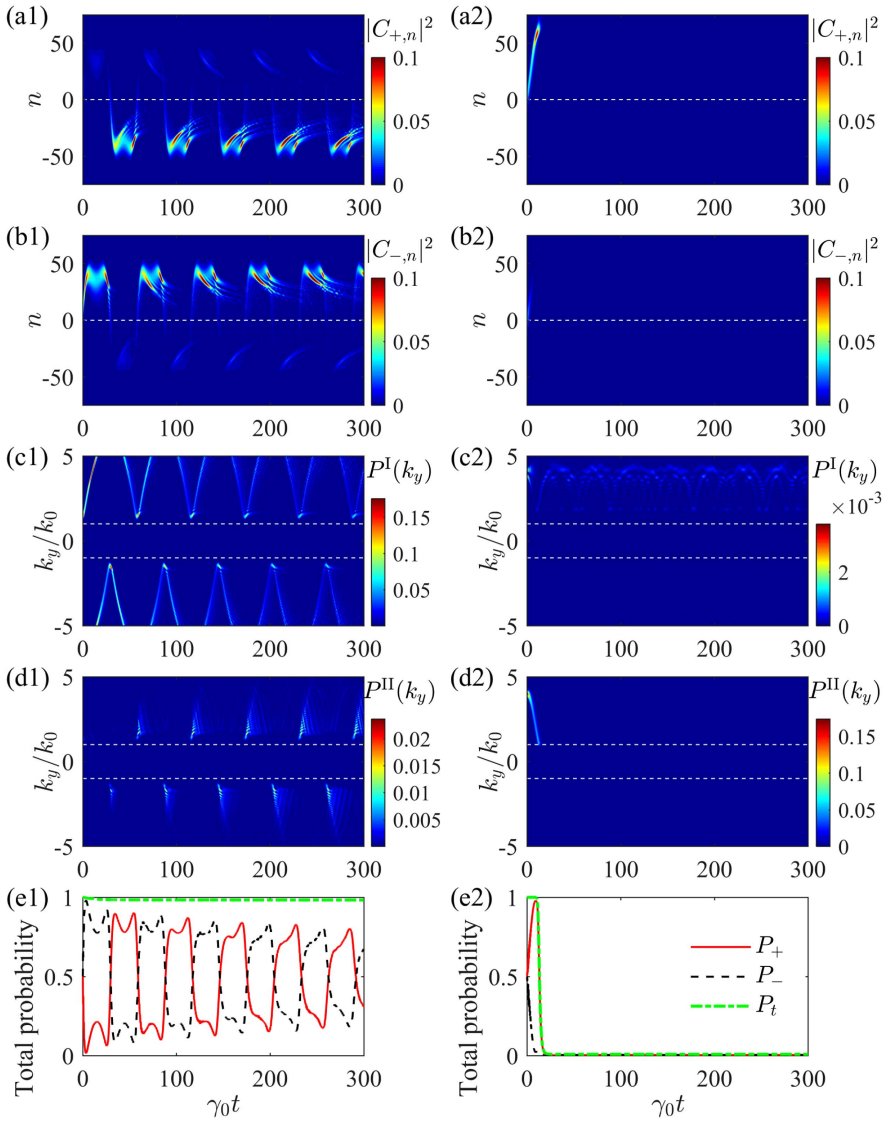

Fig. 2. Bloch oscillations for Gaussian excitations initially centered at $n_c = 0$ with $k_c = 1.5k_0$ on band I (left) and $k_c = 4k_0$ on band II (right), shown by temporal evolution for excitation probabilities of (a1), (a2) $|C_{+,n}|^2$; (b1), (b2) $|C_{-,n}|^2$; (c1), (c2) $P^{\mathrm{I}}(k_y)$; (d1), (d2) $P^{\mathrm{II}}(k_y)$; (e1), (e2) P_+, P_-, and P_t. Here, $a = 0.1\lambda$ and $\mu B_0/\hbar = 0.2\gamma_0$.

oscillation pattern with the shape of the wavepacket deforming gradually. The excitation of the $|+\rangle$ ($|-\rangle$) states in the atomic arrays is mainly located in the finite region with $y < 0$ ($y > 0$) so there is no boundary effects due to finite atoms.

We then perform fast Fourier transform (FFT) on the simulation results $C_{\pm,n}(t)$ and calculate the projection of the excited wavepacket in k_y-space onto the two bands [excitation probabilities $P^{\mathrm{I}}(k_y, t)$ and $P^{\mathrm{II}}(k_y, t)$, respectively]. Note that the Bloch band picture is valid only with constant magnetic field. Here, the linear magnetic field and resulting constant force produce perturbation, so we can calculate the projection by taking into account the uniform potentials at the value of $V_{\pm,n} = \pm\bar{n}\mu B_0$, where $\bar{n} \equiv \langle\Psi|\sum_n(|+_n\rangle n\langle+_n| + |-_n\rangle n\langle-_n|)|\Psi\rangle$ is the mean position of the wavepacket. This analysis in the Bloch band picture with uniform on-site potentials reveals dynamical features different from a conventional Bloch oscillation. Figures 2(c1) and 2(d1) show the evolution of excitation probabilities of band I and band II and P^{I} and P^{II} at each k_y. The choice of $\psi_\pm$ makes the initial excitation on band I, and throughout the evolution, P^{II} is about 1 order of magnitude smaller than P^{I}. Remarkably, one sees that P^{I} does not evolve unidirectionally on k_y with time, which gives the fundamental difference from the conventional Bloch oscillations. The evolution direction of P^{I} reverses every time (referred to as the reverse time) before it enters the free-space light cone in the k_y-axis [dash lines in Figs. 2(c1) and 2(d1)], which leads to the important consequence of avoiding a large collective decay of the excited wavepacket. We further show the total excitation probabilities of the $|+\rangle$ state and the $|-\rangle$ state (P_+, P_-) in the real space and the total excitation probability $P_t = P_+ + P_-$ in Fig. 2(e1). We find that the times when $P_+ = P_-$ are exactly the same as the reverse times because the phenomenological force $\langle F\rangle$ becomes zero and subsequently changes its direction. In other words, when the center of

the wavepacket arrives at $n = 0$, $P_+ \approx P_-$ and hence $\langle F \rangle$ changes its direction, resulting in the reverse of $P^{\mathrm{I}}(k_y)$ in the momentum space. Moreover, P_t exhibits no decay in this dissipative atomic system, which is actually lasting $\sim 10^8 \gamma_0^{-1}$ given by the simulation with a much longer evolution time. Therefore, as long as the excited wavepacket in the atomic arrays does not enter the dissipative zone inside the free-space light cone, the life time of the excitation gives the subradiant feature, which is much longer than the free-space decay time. Such extreme subradiant oscillations can be optimized by choosing initial excitations. In particular, we find that P_t can last more than $\sim 10^{13} \gamma_0^{-1}$ for an initial state centered at $k_c = 3k_0$ on band I. Based on the eigenvalue analysis of the effective Hamiltonian for an array under a linear magnetic field, one can determine the decay rate of the most subradiant eigenstate, which is consistent with the property of the optimized subradiant Bloch oscillations (see Appendix A for details).

As one may notice, the initial choice of the excited wavepacket determines how the wavepacket evolves in k_y-space and hence how the wavepacket decays. For example, if we choose $\psi_+ = 0.168$, $\psi_- = -0.168$, and $k_c = 4k_0$ to excite band I or $\psi_+ = 0.168$, $\psi_- = -0.168$, and $k_c = 2k_0$ to excite band II, we find the total probability of the wavepacket undergoes no decay even though the evolution patterns are different (see Fig. 5 in Appendix A). However, in the case of $\psi_+ = \psi_- = 0.168$ and $k_c = 4k_0$, with band II being excited, the dramatically different dynamics is as shown in Figs. 2(a2)–2(e2). One notes that the excitation undergoes a rapid decay after the partial oscillation during the initial time duration $\sim 11\gamma_0^{-1}$. The fundamental difference here is that the excitation probability P^{II} moves into the free-space light cone along the k_y-axis before $\langle F \rangle$ changes its direction. This result leads to a very fast decay within $\sim 8\gamma_0^{-1}$ for the total probability P_t dropping to ~ 0.02. In real space, the excitation on the $|-\rangle$ arm decreases fast, while the excitation on the $|+\rangle$ arm increases initially with an oscillation towards the positive y-axis but decays rapidly afterwards.

The two-band Bloch oscillation in the atomic arrays under the linear magnetic field brings unique opportunity for manipulating the decay of the excited wavepacket. For instance, we can control the collective decay exhibiting quantization-like decay with stable plateaus, as shown in Fig. 3(c1). To achieve it, we choose $\psi_+ = \psi_- = 0.168$ and $k_c = k_0$, so the wavepacket on band I centered at k_0 is initially excited. The simulation results are summarized in Figs. 3(a1)–3(c1). The wavepacket experiences decay at $t \sim 0$ because the initial wavepacket is partially inside the free-space light cone. However, the wavepacket initially moves toward the positive direction in the k_y-axis [see $P^{\mathrm{I}}(k_y) + P^{\mathrm{II}}(k_y)$ in Fig. 3(b1)], so P_t ends in a stable plateau at $t \sim 2\gamma_0^{-1}$ with a value ~ 0.67. At $t \sim 27\gamma_0^{-1}$, the excited wavepacket is reached at $k_y = -k_0$, and a reversal happens due to the change of $\langle F \rangle$, which results in a rapid drop of P_t to ~ 0.48. Periodic oscillations are exhibited, together with the oscillations of $P_n = |C_{+,n}|^2 + |C_{-,n}|^2$, in the real space. The total excitation probability P_t therefore shows the overall decay tendency with the periodic plateaus [see Fig. 3(c1)]. Initial excitations inside the free-space light cone can exhibit similar oscillations but quicker decay. Particularly, for an initial wavepacket at $k_c = -0.5k_0$ on band II, P_t decays to ~ 0.02 within

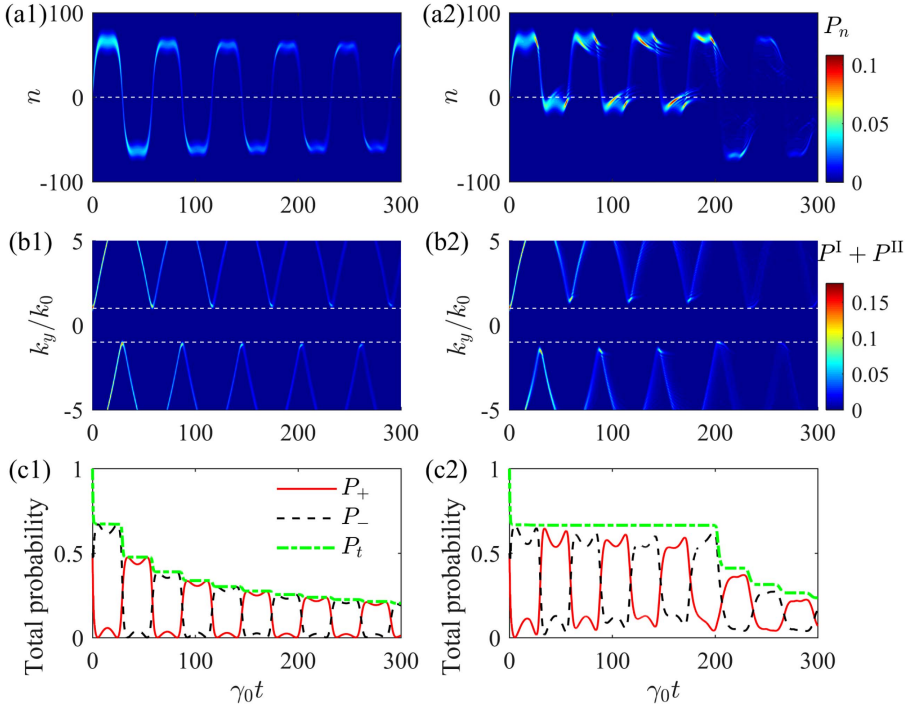

Fig. 3. Bloch oscillations for Gaussian excitations initially centered at $n_c = 0$ and $k_c = k_0$ on band I with a static magnetic field (left) and a controllable magnetic field (right), whose zero point is shifted to $y = 30a$ over a time period from 0 to $20\gamma_0^{-1}$ and back to $y = 0$ over a time period from $180\gamma_0^{-1}$ to $200\gamma_0^{-1}$, shown by temporal evolution of (a1), (a2) P_n; (b1), (b2) $P^{\mathrm{I}} + P^{\mathrm{II}}$; (c1), (c2) P_+, P_-, and P_t. Other parameters are the same as those in Fig. 2.

$t \sim 0.85\gamma_0^{-1}$, or a collective superradiant decay rate of $\sim 4.7\gamma_0$. Moreover, excitations with $n_c \neq 0$ can bring different Block oscillation phenomena because the central momenta at reverse times are changed during the evolution of the wavepacket (see Appendix A for details).

Taking advantage of the relation between reverse times and the atomic position in the linear magnetic field, one can control the momentum of the wavepacket at the reverse time. The magnetic field acts as an effective field on the single particle and breaks the spatial translation symmetry, which leads to the particle movement in the momentum space. Change of the magnetic field would alter the effective force and the momentum space evolution of the wavepacket. We give an example in Figs. 3(a2)–3(c2), where the spatial distribution of the linear magnetic field relative to the atomic position is tuned to control the evolution of the wavepacket that is initially excited at k_0 on band I [the same as that in Figs. 3(a1)–3(c1)]. In the numerical simulation, we tune the zero point of the magnetic field from $y = 0$ to $y = 30a$ over a time period from 0 to $20\gamma_0^{-1}$. As a result, after P_t drops to the first plateau, the wavepacket oscillates around the new center $y = 30a$ [Fig. 3(a2)] and reverses at $\sim \pm 1.4k_0$ in the momentum space to maintain subradiance [Fig. 3(b2)]. The excitation can also be driven to the dissipative zone by moving the zero point of the magnetic field back to $y = 0$ over a time period from $180\gamma_0^{-1}$ to $200\gamma_0^{-1}$ and decay radiatively, shown by descending plateaus in the total excitation probability.

4. DISCUSSION AND CONCLUSION

The proposed atomic arrays can be realized in various experimental systems. Dependent on different experimental platforms, atomic arrays can be composed with atom ensembles in the gas phase, such as neutral particles, including Rydberg atoms trapped in optical lattices [19,21–23,63,64] and optical tweezers [20,24–28,65–68], or atom-like particles in the solid phase, such as color defects in diamond nanophotonic devices [71,72], and excitons in atomically thin semiconductors [73]. Considering the possible imperfection of atomic positions and the inhomogeneous broadening in the atomic array, numerical results show that positional disorder suppresses the positive influence of the magnetic field on subradiance (see Appendix B for details). This limitation is expected to be overcome by the development of experimental control techniques. On the other hand, the effect of decay suppression can be found in arrays with different atomic numbers and interatomic distances to possibly decrease experimental challenges. The performance of subradiance relies on the magnitude of the linear magnetic field. The parameters used above present better initial state selections and characteristic performance of Bloch oscillations, which may further be optimized for extreme subradiance. Moreover, it has been shown recently that dispersionless or trapped subradiant photon states can be created in one-dimensional emitter chains [74]. Different from Ref. [74], our study shows that, in the model with the external magnetic field it is possible to decrease the subradiant decay rate to smaller than that in the atomic arrays without the magnetic field and also points out the possibility of quantum-state switching from the external-field control.

In summary, we have explored single-excitation dynamics in 1D atomic arrays under a linear magnetic field. Resulting two-band Bloch oscillations are studied. We found that the evolution of the wavepacket in the momentum space depends on the phenomenological force $\langle F \rangle$, which is determined by local properties of the band structure and thus influenced by the position of the wavepacket in the real space. Compared to the conventional Bloch oscillations, the evolution direction of the momentum reverses as long as the wavepacket passes the position where $\langle F \rangle$ changes its sign. Taking advantage of this unique property, we show the capability of generating exotic subradiant oscillations that lasts orders of magnitude greater than the atomic spontaneous decay time. Our study takes advantage of the external control from the magnetic field and therefore points toward fundamental opportunities in switching quantum states between superradiant and subradiant states and realizing an extreme subradiant quantum state that could be useful in important applications for quantum storage.

APPENDIX A: BLOCH OSCILLATIONS FOR DIFFERENT INITIAL STATES

Here, we show more studies with different parameters in atomic arrays with an interatomic distance $a = 0.1\lambda$. We perform simulations for a much longer evolution time with initial parameters $\psi_+ = \psi_- = 0.168$ and $k_c = 1.5k_0$ to excite band I. The excitation probabilities of each atom $P_n(t) = |C_{+,n}(t)|^2 + |C_{-,n}(t)|^2$ and in the momentum space $P^{\mathrm{I}}(k_y, t) + P^{\mathrm{II}}(k_y, t)$ of an $N = 201$ atomic array are shown in Figs. 4(a1) and 4(b1), respectively, for a period of $300\gamma_0^{-1}$ after $t = 10^8\gamma_0^{-1}$. Oscillations for the excitation last $\sim 10^8\gamma_0^{-1}$, though the wavepacket has dispersed. The excitation wavepacket avoids entering the dissipative zone and largely stays on band I in the momentum space. Furthermore, we plot the evolution of total excitation probabilities for different numbers of atoms in Fig. 4(c1). With parameters initiating subradiant Bloch oscillations, the subradiant life time does not change with the atomic number of long arrays due to the spatial confinement of the oscillations. When the length of the atomic array is comparable to the extended region of the Bloch oscillations, the life time decreases rapidly due to scattering at each end of the finite array.

We plot simulations for another initial state of $\psi_+ = 0.168$, $\psi_- = -0.168$, and $k_c = 3k_0$ to excite band I in Figs. 4(a2)–4(c2), which gives an optimum life time of Bloch oscillations over 13 orders of magnitude greater than the atomic spontaneous decay time. $P_n(t)$ in Fig. 4(a2) and $P^{\mathrm{I}}(k_y, t) + P^{\mathrm{II}}(k_y, t)$ in Fig. 4(b2) of an $N = 201$ atomic array show more confined oscillations in both the real space and the momentum space, for a period of $300\gamma_0^{-1}$ after $t = 10^{13}\gamma_0^{-1}$. The life time of the excitation drops significantly only for a small atomic number $N = 51$.

If we choose $\psi_+ = 0.168$, $\psi_- = -0.168$, and $k_c = 4k_0$ to excite band I [Figs. 5(a1)–5(c1)] or $\psi_+ = 0.168$, $\psi_- = -0.168$, and $k_c = 2k_0$ to excite band II [Figs. 5(a2)–5(c2)], then we find the total probability of the wavepacket undergoes almost no decay even though the evolution patterns are different. In the momentum space, the wavepacket reverses and oscillates around the degenerate point $k_y \sim 2.3k_0$ in the band

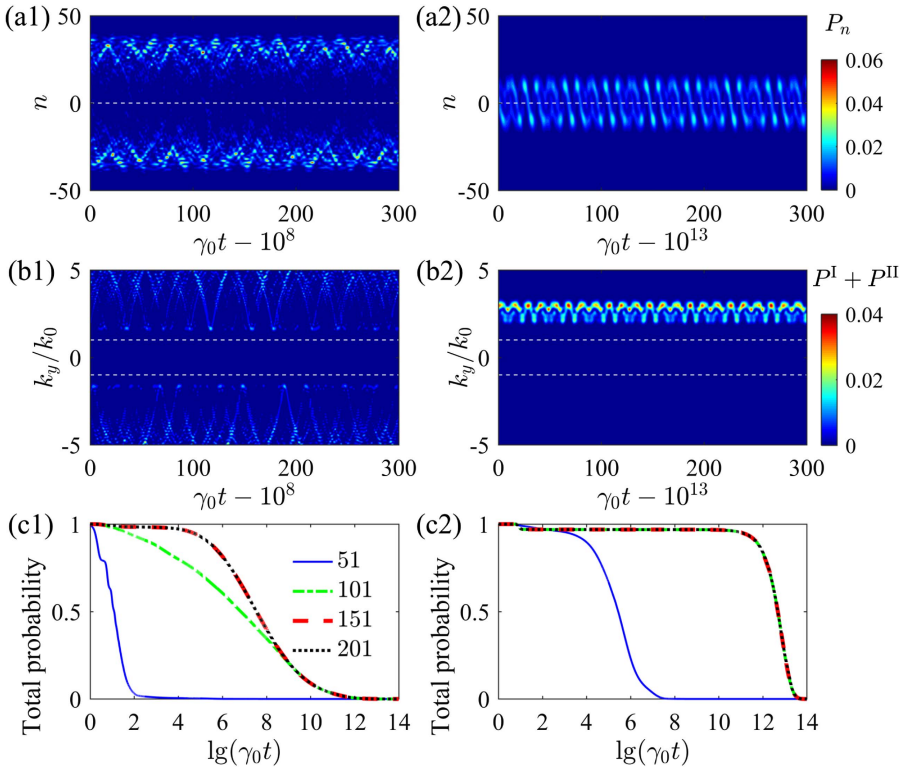

Fig. 4. Bloch oscillations for a Gaussian excitation initially centered at $n_c = 0$ with $k_c = 1.5k_0$ (left) and $k_c = 3k_0$ (right) on band I. Temporal evolution of (a1), (a2) $P_n = |C_{+,n}|^2 + |C_{-,n}|^2$ and (b1), (b2) $P^{\mathrm{I}}(k_y) + P^{\mathrm{II}}(k_y)$ in an array with atomic number $N = 201$ within a time period of $300\,\gamma_0^{-1}$ after $t = 10^8\,\gamma_0^{-1}$ (left) and after $t = 10^{13}\,\gamma_0^{-1}$ (right). (c1), (c2) The total probability P_t versus order of magnitude of time for $N = 51$ (blue solid line), $N = 101$ (green dash-dotted line), $N = 151$ (red dash line), and $N = 201$ (black dotted line). $a = 0.1\lambda$ and $\mu B_0/\hbar = 0.2\gamma_0$.

structure without the magnetic field and thus experiences slow dissipation.

Initial excitations inside the free-space light cone exhibit quick decay. Figures 5(a3)–5(c3) show results for an initial wavepacket at $k_c = -0.5k_0$ on band II. P_t decays to ~0.02 within $t \sim 0.85\gamma_0^{-1}$, which is fitted with an exponential decay function $e^{-4.7\gamma_0 t}$.

Next, we consider excitations with $n_c \neq 0$. We find that when n_c is close to 0, similar phenomena shown above can be found. When n_c is far away from 0, Bloch oscillation

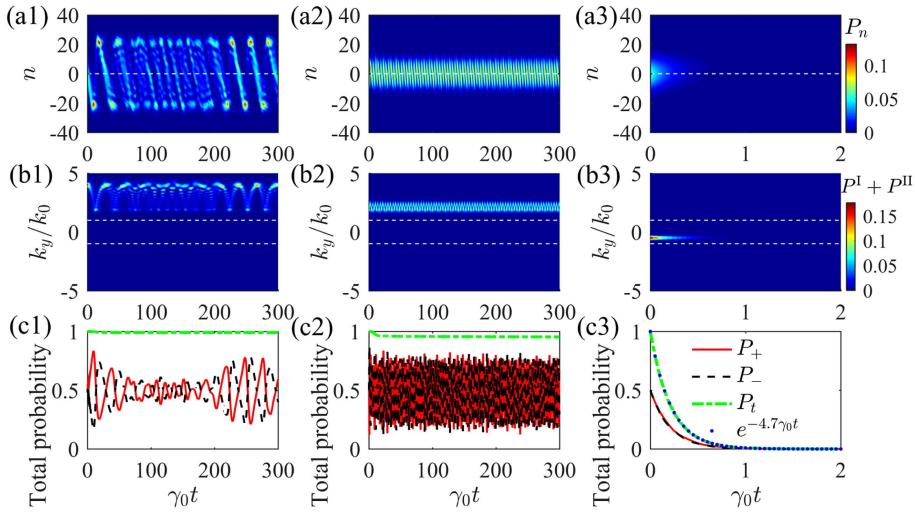

Fig. 5. Bloch oscillations started from $n_c = 0$ for Gaussian excitations initially centered at $k_c = 4k_0$ on band I (left), $k_c = 2k_0$ on band II (middle), and $k_c = -0.5k_0$ on band II (right), shown by temporal evolutions of (a1)–(a3) P_n, (b1)–(b3) $P^{\mathrm{I}}(k_y) + P^{\mathrm{II}}(k_y)$, (c1), (c2) total excitation probabilities P_+ (red solid line), P_- (black dash line), and P_t (green dash-dotted line). An exponential function is used to fit the decay of the total excitation probability in (c3) (blue dotted line). Here, $N = 201$, $a = 0.1\lambda$, and $\mu B_0/\hbar = 0.2\gamma_0$.

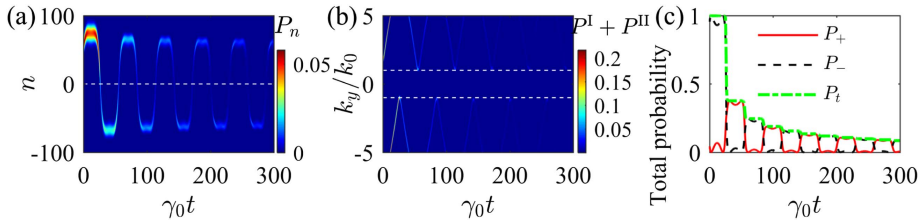

Fig. 6. Bloch oscillations started from $n_c = 50$ for a Gaussian excitation initially centered at $k_c = 1.5k_0$ on band I, shown by the temporal evolution of (a) P_n, (b) $P^{\mathrm{I}} + P^{\mathrm{II}}$, (c) P_+ (red solid line), P_- (black dash line), and P_t (green dash-dotted line). Here $N = 201$, $a = 0.1\lambda$, and $\mu B_0/\hbar = 0.2\gamma_0$.

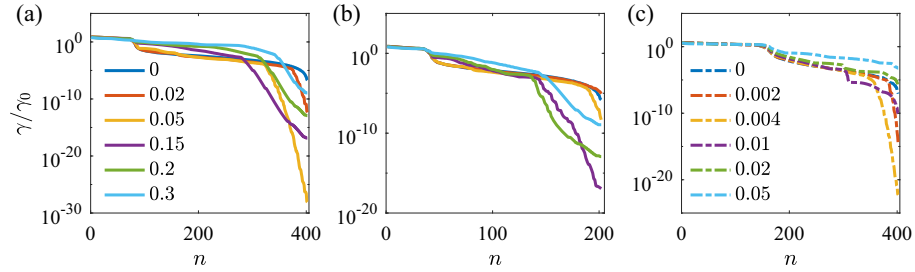

Fig. 7. Numerically calculated decay rates in descending order of single-excitation eigenstates in an atomic array under a linear magnetic field with varying $\mu B_0/\hbar\gamma_0$ indicated by different colors for (a) $a = 0.1\lambda$, $N = 201$; (b) $a = 0.1\lambda$, $N = 101$; and (c) $a = 0.2\lambda$, $N = 201$.

phenomena deviate from the cases with $n_c = 0$ if the same initial momentum k_c is taken. The reason is that during the evolution of the wavepacket, the central momenta at reverse times change compared to cases with $n_c = 0$, which leads to a different evolution pattern in the momentum space. As an example, we show the simulation results in Fig. 6 with $\psi_+ = 0.0502$, $\psi_- = 0.232$, $k_c = 1.5k_0$, and $n_c = 50$ to excite band I. Compared with simulations in Figs. 2(a1)–2(e1) in the main text, the difference here is that the center of the excited wavepacket moves from 0 to $50a$. The wavepacket evolution shows periodic oscillations with gradual reduction of the amplitude in the real space. From Fig. 6(b), one can see the momenta at reverse times are around $k_y = \pm k_0$, which leads to the decay of the total probability with periodic plateaus, as shown in Fig. 6(c). This phenomenon is similar to the case with $n_c = 0$ and the initial momentum $k_c = k_0$ in Figs. 3(a1)–3(c1) in the main text. Larger deviation from the center in the initial excitation with $k_c = 1.5k_0$ can cause the wavepacket to evolve into the dissipative zone further and exhibit quicker decay.

APPENDIX B: DECAY RATES OF SINGLE-EXCITATION EIGENSTATES

We give an analysis of decay rates of collective eigenstates in atomic arrays and their dependence on the linear magnetic field. For the interatomic distance and atomic number considered in the main text [Fig. 7(a)], lower decay rates can be achieved by applying the linear magnetic field. The most subradiant decay rate reduces as B_0 increases to $\sim 0.05\hbar\gamma_0/\mu$ and then rises. Numerical results determine that the decay rates of the most subradiant states are $\gamma = 8.1 \times 10^{-29}$ for $B_0 = 0.05\hbar\gamma_0/\mu$ and $\gamma = 1.2 \times 10^{-13}$ for $B_0 = 0.2\hbar\gamma_0/\mu$. For shorter atomic arrays with $N = 101$ in Fig. 7(b), larger magnetic field gradients cause similar effects, but small magnetic field gradients have limited influences on the decay rate suppression. Variation of interatomic distance causes more evident changes of single-excitation eigenstates. For $a = 0.2\lambda$ and $N = 201$ in Fig. 7(c), the positive influence of the magnetic field on the decay rate suppression is limited to very small magnetic field gradients. Large magnetic field gradients give rise to increased collective decay rates and the lifetimes of subradiant states noticeably decrease.

Here, we briefly discuss the effect of positional disorder and inhomogeneous broadening on single-excitation collective decay rates. The deviations of emitter positions from an ideal array are modeled by randomly placing the atom within a width of δa from each lattice site along the y-axis. We plot the most subradiant single-excitation decay rate in an atomic array with increasing disorder in Fig. 8(a). Without the external magnetic field, the subradiant decay rates noticeably increase after $\delta a/a$ reaches 10^{-2}. Under a linear magnetic field with $B_0 = 0.2\hbar\gamma_0/\mu$, the almost perfect array supports extreme subradiant states with decay rates $\sim 10^{-13}\gamma_0$, which is much lower than the case without the magnetic field. However, a slight disorder of $\delta a/a \sim 10^{-6}$ starts to weaken the subradiant effect. A disorder of $\delta a/a > 10^{-3}$ suppresses the positive influence of the magnetic field on the subradiance and leads to larger decay rates than the case without the magnetic field. We also model the Doppler shifts approximately by setting a random frequency shift of each atom according to a Gaussian probability distribution of width Δ_D and neglecting the spatial movement of atoms, as shown in Fig. 8(b). The increasing of decay rates

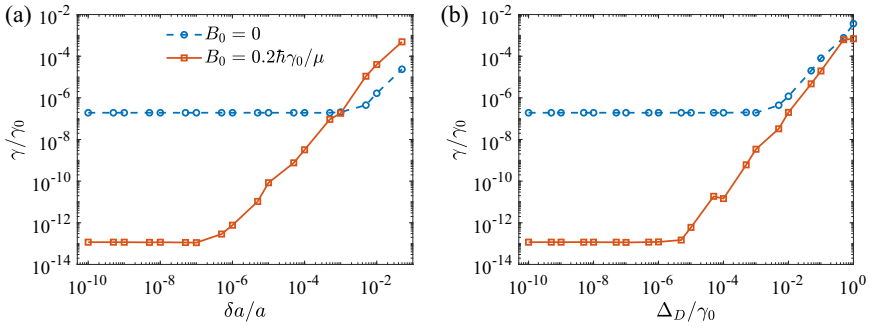

Fig. 8. Decay rates of the most subradiant single-excitation modes with (a) increasing spatial disorder characterized by the deviation width δa and (b) increasing Doppler broadening Δ_D for $B_0 = 0$ (blue dash line) and $B_0 = 0.2\hbar\gamma_0/\mu$ (red solid line). $a = 0.1\lambda$ and $N = 201$.

starts with smaller Doppler shifts in arrays with the magnetic field.

Funding. National Natural Science Foundation of China (12204304); National Key Research and Development Program of China (2021YFA1400900, 2023YFA1407200).

Acknowledgment. L.Y. thanks the sponsorship from the Yangyang Development Fund.

Disclosures. The authors declare no conflicts of interest.

Data Availability. All data from this study are available from the corresponding authors upon reasonable request.

REFERENCES

1. K. Hammerer, A. S. Sørensen, and E. S. Polzik, "Quantum interface between light and atomic ensembles," Rev. Mod. Phys. **82**, 1041–1093 (2010).
2. V. Giovannetti, S. Lloyd, and L. Maccone, "Advances in quantum metrology," Nat. Photonics **5**, 222–229 (2011).
3. B. Olmos, D. Yu, Y. Singh, *et al.*, "Long-range interacting many-body systems with alkaline-earth-metal atoms," Phys. Rev. Lett. **110**, 143602 (2013).
4. A. González-Tudela, C.-L. Hung, D. E. Chang, *et al.*, "Subwavelength vacuum lattices and atom–atom interactions in two-dimensional photonic crystals," Nat. Photonics **9**, 320–325 (2015).
5. R. T. Sutherland and F. Robicheaux, "Collective dipole-dipole interactions in an atomic array," Phys. Rev. A **94**, 013847 (2016).
6. A. Asenjo-Garcia, M. Moreno-Cardoner, A. Albrecht, *et al.*, "Exponential improvement in photon storage fidelities using subradiance and "selective radiance" in atomic arrays," Phys. Rev. X **7**, 031024 (2017).
7. E. Shahmoon, D. S. Wild, M. D. Lukin, *et al.*, "Cooperative resonances in light scattering from two-dimensional atomic arrays," Phys. Rev. Lett. **118**, 113601 (2017).
8. B. X. Wang and C. Y. Zhao, "Topological photonic states in one-dimensional dimerized ultracold atomic chains," Phys. Rev. A **98**, 023808 (2018).
9. M. T. Manzoni, M. Moreno-Cardoner, A. Asenjo-Garcia, *et al.*, "Optimization of photon storage fidelity in ordered atomic arrays," New J. Phys. **20**, 083048 (2018).
10. D. E. Chang, J. S. Douglas, A. González-Tudela, *et al.*, "Colloquium: quantum matter built from nanoscopic lattices of atoms and photons," Rev. Mod. Phys. **90**, 031002 (2018).
11. Y.-X. Zhang and K. Mølmer, "Theory of subradiant states of a one-dimensional two-level atom chain," Phys. Rev. Lett. **122**, 203605 (2019).
12. D. F. Kornovan, N. V. Corzo, J. Laurat, *et al.*, "Extremely subradiant states in a periodic one-dimensional atomic array," Phys. Rev. A **100**, 063832 (2019).
13. P.-O. Guimond, A. Grankin, D. V. Vasilyev, *et al.*, "Subradiant Bell states in distant atomic arrays," Phys. Rev. Lett. **122**, 093601 (2019).
14. R. Bekenstein, I. Pikovski, H. Pichler, *et al.*, "Quantum metasurfaces with atom arrays," Nat. Phys. **16**, 1 (2020).
15. Y.-X. Zhang and K. Mølmer, "Subradiant emission from regular atomic arrays: universal scaling of decay rates from the generalized Bloch theorem," Phys. Rev. Lett. **125**, 253601 (2020).
16. B. X. Wang and C. Y. Zhao, "Topological quantum optical states in quasiperiodic cold atomic chains," Phys. Rev. A **103**, 013727 (2021).
17. K. E. Ballantine and J. Ruostekoski, "Quantum single-photon control, storage, and entanglement generation with planar atomic arrays," PRX Quantum **2**, 040362 (2021).
18. O. Rubies-Bigorda, V. Walther, T. L. Patti, *et al.*, "Photon control and coherent interactions via lattice dark states in atomic arrays," Phys. Rev. Res. **4**, 013110 (2022).
19. J. Zeiher, J.-Y. Choi, A. Rubio-Abadal, *et al.*, "Coherent many-body spin dynamics in a long-range interacting Ising chain," Phys. Rev. X **7**, 041063 (2017).
20. S. de Léséleuc, V. Lienhard, P. Scholl, *et al.*, "Observation of a symmetry-protected topological phase of interacting bosons with Rydberg atoms," Science **365**, 775–780 (2019).
21. T. M. Graham, M. Kwon, B. Grinkemeyer, *et al.*, "Rydberg-mediated entanglement in a two-dimensional neutral atom qubit array," Phys. Rev. Lett. **123**, 230501 (2019).
22. A. Glicenstein, G. Ferioli, N. Šibalić, *et al.*, "Collective shift in resonant light scattering by a one-dimensional atomic chain," Phys. Rev. Lett. **124**, 253602 (2020).
23. J. Rui, D. Wei, A. Rubio-Abadal, *et al.*, "A subradiant optical mirror formed by a single structured atomic layer," Nature **583**, 369–374 (2020).
24. D. Bluvstein, A. Omran, H. Levine, *et al.*, "Controlling quantum many-body dynamics in driven Rydberg atom arrays," Science **371**, 1355–1359 (2021).
25. S. Ebadi, T. T. Wang, H. Levine, *et al.*, "Quantum phases of matter on a 256-atom programmable quantum simulator," Nature **595**, 227–232 (2021).
26. G. Semeghini, H. Levine, A. Keesling, *et al.*, "Probing topological spin liquids on a programmable quantum simulator," Science **374**, 1242–1247 (2021).
27. D. Bluvstein, H. Levine, G. Semeghini, *et al.*, "A quantum processor based on coherent transport of entangled atom arrays," Nature **604**, 451–456 (2022).
28. S. Ebadi, A. Keesling, M. Cain, *et al.*, "Quantum optimization of maximum independent set using Rydberg atom arrays," Science **376**, 1209–1215 (2022).
29. A. A. Svidzinsky, J.-T. Chang, and M. O. Scully, "Cooperative spontaneous emission of N atoms: many-body eigenstates, the effect of virtual Lamb shift processes, and analogy with radiation of N classical oscillators," Phys. Rev. A **81**, 053821 (2010).

30. A. Tiranov, V. Angelopoulou, C. J. van Diepen, *et al.*, "Collective super- and subradiant dynamics between distant optical quantum emitters," Science **379**, 389–393 (2023).
31. A. Browaeys and T. Lahaye, "Many-body physics with individually controlled Rydberg atoms," Nat. Phys. **16**, 132–142 (2020).
32. H. H. Jen, M.-S. Chang, and Y.-C. Chen, "Cooperative single-photon subradiant states," Phys. Rev. A **94**, 013803 (2016).
33. D. Plankensteiner, L. Ostermann, H. Ritsch, *et al.*, "Selective protected state preparation of coupled dissipative quantum emitters," Sci. Rep. **5**, 16231 (2015).
34. G. Facchinetti, S. D. Jenkins, and J. Ruostekoski, "Storing light with subradiant correlations in arrays of atoms," Phys. Rev. Lett. **117**, 243601 (2016).
35. K. E. Ballantine and J. Ruostekoski, "Subradiance-protected excitation spreading in the generation of collimated photon emission from an atomic array," Phys. Rev. Res. **2**, 023086 (2020).
36. J. A. Needham, I. Lesanovsky, and B. Olmos, "Subradiance-protected excitation transport," New J. Phys. **21**, 073061 (2019).
37. J. Perczel, J. Borregaard, D. E. Chang, *et al.*, "Topological quantum optics in two-dimensional atomic arrays," Phys. Rev. Lett. **119**, 023603 (2017).
38. J. Perczel, J. Borregaard, D. E. Chang, *et al.*, "Photonic band structure of two-dimensional atomic lattices," Phys. Rev. A **96**, 063801 (2017).
39. R. J. Bettles, J. Minář, C. S. Adams, *et al.*, "Topological properties of a dense atomic lattice gas," Phys. Rev. A **96**, 041603 (2017).
40. S. Weber, S. de Léséleuc, V. Lienhard, *et al.*, "Topologically protected edge states in small Rydberg systems," Quantum Sci. Technol. **3**, 044001 (2018).
41. A. Zhang, L. Wang, X. Chen, *et al.*, "Tunable super- and subradiant boundary states in one-dimensional atomic arrays," Commun. Phys. **2**, 157 (2019).
42. J. Perczel, J. Borregaard, D. E. Chang, *et al.*, "Topological quantum optics using atomlike emitter arrays coupled to photonic crystals," Phys. Rev. Lett. **124**, 083603 (2020).
43. T.-H. Yang, B.-Z. Wang, X.-C. Zhou, *et al.*, "Quantum Hall states for Rydberg arrays with laser-assisted dipole-dipole interactions," Phys. Rev. A **106**, L021101 (2022).
44. G. Facchinetti and J. Ruostekoski, "Interaction of light with planar lattices of atoms: reflection, transmission, and cooperative magnetometry," Phys. Rev. A **97**, 023833 (2018).
45. J. Javanainen and R. Rajapakse, "Light propagation in systems involving two-dimensional atomic lattices," Phys. Rev. A **100**, 013616 (2019).
46. M. A. N. Gisin and H. de Riedmatten, "Quantum memory for photons," Phys. Today **68**, 42–47 (2015).
47. S. Longhi, "Bloch oscillations in complex crystals with PT symmetry," Phys. Rev. Lett. **103**, 123601 (2009).
48. M. Atala, M. Aidelsburger, J. T. Barreiro, *et al.*, "Direct measurement of the Zak phase in topological Bloch bands," Nat. Phys. **9**, 795–800 (2013).
49. G. Jotzu, M. Messer, R. Desbuquois, *et al.*, "Experimental realization of the topological Haldane model with ultracold fermions," Nature **515**, 237–240 (2014).
50. Y. Ke, X. Qin, H. Zhong, *et al.*, "Bloch-Landau-Zener dynamics in single-particle Wannier-Zeeman systems," Phys. Rev. A **91**, 053409 (2015).
51. R. Khomeriki and S. Flach, "Landau-Zener Bloch oscillations with perturbed flat bands," Phys. Rev. Lett. **116**, 245301 (2016).
52. Y. V. Kartashov, V. V. Konotop, D. A. Zezyulin, *et al.*, "Bloch oscillations in optical and Zeeman lattices in the presence of spin-orbit coupling," Phys. Rev. Lett. **117**, 215301 (2016).
53. Y. Zheng, S. Feng, and S.-J. Yang, "Chiral Bloch oscillation and nontrivial topology in a ladder lattice with magnetic flux," Phys. Rev. A **96**, 063613 (2017).
54. X. Qiao, X.-B. Zhang, A.-X. Zhang, *et al.*, "Dynamics and phase transitions in biased ladder systems with magnetic flux," Phys. Lett. A **383**, 3095–3100 (2019).
55. W. Ji, K. Zhang, W. Zhang, *et al.*, "Bloch oscillations of spin-orbit-coupled cold atoms in an optical lattice and spin-current generation," Phys. Rev. A **99**, 023604 (2019).
56. A. Regensburger, C. Bersch, M.-A. Miri, *et al.*, "Parity–time synthetic photonic lattices," Nature **488**, 167–171 (2012).
57. L. Yuan and S. Fan, "Bloch oscillation and unidirectional translation of frequency in a dynamically modulated ring resonator," Optica **3**, 1014–1018 (2016).
58. Y. Zhang, D. Zhang, Z. Zhang, *et al.*, "Optical Bloch oscillation and Zener tunneling in an atomic system," Optica **4**, 571–575 (2017).
59. M. O. Scully, "Single photon subradiance: quantum control of spontaneous emission and ultrafast readout," Phys. Rev. Lett. **115**, 243602 (2015).
60. Z. Wang, H. Li, W. Feng, *et al.*, "Controllable switching between superradiant and subradiant states in a 10-qubit superconducting circuit," Phys. Rev. Lett. **124**, 013601 (2020).
61. D. Ferraro, M. Campisi, G. M. Andolina, *et al.*, "High-power collective charging of a solid-state quantum battery," Phys. Rev. Lett. **120**, 117702 (2018).
62. G. M. Andolina, M. Keck, A. Mari, *et al.*, "Extractable work, the role of correlations, and asymptotic freedom in quantum batteries," Phys. Rev. Lett. **122**, 047702 (2019).
63. A. Kumar, T. Y. Wu, F. Giraldo, *et al.*, "Sorting ultracold atoms in a three-dimensional optical lattice in a realization of Maxwell's demon," Nature **561**, 83–87 (2018).
64. D. O. de Mello, D. Schäffner, J. Werkmann, *et al.*, "Defect-free assembly of 2D clusters of more than 100 single-atom quantum systems," Phys. Rev. Lett. **122**, 203601 (2019).
65. D. Barredo, S. de Léséleuc, V. Lienhard, *et al.*, "An atom-by-atom assembler of defect-free arbitrary two-dimensional atomic arrays," Science **354**, 1021–1023 (2016).
66. M. Endres, H. Bernien, A. Keesling, *et al.*, "Atom-by-atom assembly of defect-free one-dimensional cold atom arrays," Science **354**, 1024–1027 (2016).
67. A. Cooper, J. P. Covey, I. S. Madjarov, *et al.*, "Alkaline-earth atoms in optical tweezers," Phys. Rev. X **8**, 041055 (2018).
68. C. Sheng, J. Hou, X. He, *et al.*, "Defect-free arbitrary-geometry assembly of mixed-species atom arrays," Phys. Rev. Lett. **128**, 083202 (2022).
69. Y. He, L. Ji, Y. Wang, *et al.*, "Geometric control of collective spontaneous emission," Phys. Rev. Lett. **125**, 213602 (2020).
70. T. Hartmann, F. Keck, H. J. Korsch, *et al.*, "Dynamics of Bloch oscillations," New J. Phys. **6**, 2 (2004).
71. A. Sipahigil, R. E. Evans, D. D. Sukachev, *et al.*, "An integrated diamond nanophotonics platform for quantum-optical networks," Science **354**, 847–850 (2016).
72. F. Casola, T. van der Sar, and A. Yacoby, "Probing condensed matter physics with magnetometry based on nitrogen-vacancy centres in diamond," Nat. Rev. Mater. **3**, 17088 (2018).
73. T. Wang, Z. Li, Y. Li, *et al.*, "Giant valley-polarized Rydberg excitons in monolayer WSe_2 revealed by magneto-photocurrent spectroscopy," Nano Lett. **20**, 7635–7641 (2020).
74. M. Cech, I. Lesanovsky, and B. Olmos, "Dispersionless subradiant photon storage in one-dimensional emitter chains," arXiv, arXiv:2303.13564 (2023).